Ring vaccination strategy in networks: A mixed percolation approach

Lautaro Vassallo [1,*] Matías A. Di Muro,[1] Debmalya Sarkar [2] Lucas D. Valdez [3] and Lidia A. Braunstein [1,3]

[1]*Instituto de Investigaciones Físicas de Mar del Plata (IFIMAR-CONICET) and Departamento de Física,*
Facultad de Ciencias Exactas y Naturales, Universidad Nacional de Mar del Plata, 7600 Mar del Plata, Argentina
[2]*Department of Information and Communication Technology, Manipal Institute of Technology,*
Manipal Academy of Higher Education, Manipal 576104, India
[3]*Physics Department, Boston University, Boston, Massachusetts 02215, USA*

Ring vaccination is a mitigation strategy that consists in seeking and vaccinating the contacts of a sick patient, in order to provide immunization and halt the spread of disease. We study an extension of the susceptible-infected-recovered (SIR) epidemic model with ring vaccination in complex and spatial networks. Previously, a correspondence between this model and a link percolation process has been established, however, this is only valid in complex networks. Here, we propose that the SIR model with ring vaccination is equivalent to a mixed percolation process of links and nodes, which offers a more complete description of the process. We verify that this approach is valid in both complex and spatial networks, the latter being built according to the Waxman model. This model establishes a distance-dependent cost of connection between individuals arranged in a square lattice. We determine the epidemic-free regions in a phase diagram based on the wiring cost and the parameters of the epidemic model (vaccination and infection probabilities and recovery time). In addition, we find that for long recovery times this model maps into a pure node percolation process, in contrast to the SIR model without ring vaccination, which maps into link percolation.

I. INTRODUCTION

The health of the population is one of the major concerns of governments and international health agencies globally. As reported by the World Health Organization, 7.5 trillion dollars was spent on health in 2016, equivalent to approximately 10% of the global gross domestic product [1]. In addition to the thousands of new pathogens discovered in the last decades, the reemergence of infectious diseases such as cholera, plague, and yellow fever is concerning [2]. Changes in lifestyles, coupled with environmental and biological changes, cause epidemics of infectious diseases to be more likely to occur and to spread farther and faster than ever before [2]. For this reason, significant efforts must be devoted to the study and control of infectious diseases, and the design of effective prevention and mitigation strategies is crucial.

Complex networks [3–6] have proven to be an important tool in the study of the spread of epidemics since they capture some features of human societies [7–10]. The nodes of a complex network represent individuals, while links represent interactions between them. In an epidemic model, the nodes adopt different states, such as susceptible or infected, while the links allow contagion between the nodes. This approach is useful when physical contact is the main route of transmission [11,12]. Epidemic models can be tested on networks with different topologies, which would represent different social structures, and in these models, the impact of different mitigation strategies, such as quarantine [13–15],

isolation [13,14,16,17], and vaccination [16,18–22], can be estimated.

In remote times, diseases spread as a diffusive process [23], while nowadays, due to modern means of transport, they can cover long distances in short times and be superdiffusive [24]. A model that allows weighting both behaviors is the Waxman model [25,26], which takes the distance-dependent cost into account when establishing connections between nodes (see Sec. IV). This model captures the fact that human interactions have a cost, such as time travel, which makes short-range interactions more frequent than long-range interactions. A wiring cost is also present in several other complex structures such as neural [27,28], telecommunication [29], Internet [30], and electricity networks [31]. Recently, the Waxman model was used to study the effects of the wiring cost on the universality of critical phenomena [32]. A network built according to this model coincides with the Erdös-Rényi (ER) network [33] if the wiring cost tends to 0, which has a Poisson degree distribution of contacts.

An epidemic model that is commonly used is the susceptible-infected-recovered (SIR) model [34–37], which reproduces the spread of nonrecurrent diseases such as influenza and SARS [38]. In this compartmental model, nodes can be in three possible states: susceptible (S), infected (I), or recovered (R). When susceptible nodes are in contact with infected ones, they may become ill with probability β. Infected individuals recover after a period of time t_r, remaining in this state as they acquire immunity against the disease. In the final state, there are only individuals in the S or R compartment. The fraction of recovered individuals R indicates the extent of the epidemic. The effective probability of transmission of the

*lvassallo@mdp.edu.ar

disease between an infected node and one of its susceptible neighbors, which is called the transmissibility, is defined as the probability of infection up to a time t_r and is given by $T = 1 - (1 - \beta)^{t_r}$. The fraction R undergoes a second-order phase transition at a critical transmissibility value T_c. If $T \leq T_c$, the cluster formed by recovered nodes in the final state is negligible (epidemic-free phase), but it has a size of the order of the entire population for $T > T_c$ (epidemic phase). It has been shown that the SIR model maps into link percolation if the probability of link occupation, i.e., the control parameter, is $p_L = T$. In this way, the fraction of recovered nodes maps into the fraction P_∞ of nodes that belong to the giant component (GC) of the link percolation process, i.e., the order parameter. This correspondence was first observed in lattices in [39] and then extended to complex networks [35].

Several strategies can be carried out to prevent or mitigate the impact of a disease. Among these, ring vaccination has proven effective in the containment of epidemics [40,41]. It consists in tracing and vaccinating the close contacts of a sick patient, to surround the disease and prevent its spread. It was first implemented against smallpox [42,43], which greatly aided its eradication in 1980, and is currently being used to treat Ebola outbreaks in the Democratic Republic of the Congo, with encouraging results [44]. The SIR model can be extended to study the ring vaccination strategy by adding a fourth compartment: vaccinated nodes (V). Within the context of complex networks, the susceptible-infected-vaccinated-recovered (SIR-V) model was tested in single and partially overlapping multiplex networks [45,46]. In [45] it was shown that the sum of the fraction of recovered and vaccinated nodes, $R + V$, map into the fraction of nodes that belongs to the GC in link percolation.

However, the equivalence between the SIR-V model and link percolation stated in the previous references is not general, as it only holds for complex networks. Moreover, in link percolation, there is no clear distinction between nodes associated with recovered and nodes associated with vaccinated individuals. In this study, we propose a more general percolation process which provides a more complete description and understanding of the SIR-V model. We show that the fraction of recovered nodes R maps into the relative size of the GC of a mixed percolation process [47,48], where both edges and nodes may be "occupied-unoccupied" with independent probabilities, i.e., there are two control parameters. We use the generating function formalism for complex networks to derive the theoretical equations for R and V, separately, and numerically verify that the mapping holds in Waxman spatial networks. Furthermore, we study the effect of the wiring cost on the epidemic threshold.

II. EPIDEMIC MODEL AND MAPPING INTO MIXED PERCOLATION

The SIR-V model with ring vaccination is an extension of the original SIR model. In this model, at each time step, a susceptible node that is in contact with an infected one is first immunized with probability ω. Thus, the probability of infection at each time step is $(1 - \omega)\beta$. The rules of the model

are the following:

$$S + I \xrightarrow{\omega} V + I, \tag{1a}$$

$$S + I \xrightarrow{(1-\omega)\beta} I + I, \tag{1b}$$

$$I \xrightarrow{t_r} R, \tag{1c}$$

where t_r is the recovery time.

The effective probability of transmission of the disease T_β through an active link, i.e., a link between an infected node and its susceptible neighbor, is now given by

$$
\begin{aligned}
T_\beta &= (1 - \omega)\beta \sum_{t=1}^{t_r} [(1 - \omega)(1 - \beta)]^{t-1} \\
&= \frac{1 - (1 - \omega)^{t_r}(1 - \beta)^{t_r}}{(1 - \omega)\beta + \omega}(1 - \omega)\beta. \tag{2}
\end{aligned}
$$

This expression accounts for the probability of a node being infected at any time by an infected neighbor, given that it was not infected or vaccinated at prior times. In particular, for $\omega = 0$, T_β corresponds to the transmissibility T of the SIR model.

Similarly, the effective probability of vaccination T_ω is given by

$$
\begin{aligned}
T_\omega &= \omega \sum_{t=1}^{t_r} [(1 - \omega)(1 - \beta)]^{t-1} \\
&= \frac{1 - (1 - \omega)^{t_r}(1 - \beta)^{t_r}}{(1 - \omega)\beta + \omega}\omega. \tag{3}
\end{aligned}
$$

The first two rules of the epidemic model, (1a) and (1b), are equivalent to the following transition rule:

$$
S + I \xrightarrow{(1-\omega)\beta+\omega} \Delta + I \xrightarrow{\quad C_\beta \quad} I + I
$$
$$
\searrow^{C_\omega}
$$
$$
V + I \tag{4}
$$
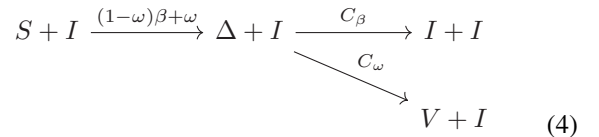
where $C_\beta = \frac{T_\beta}{T_\beta + T_\omega}$ and $C_\omega = 1 - C_\beta = \frac{T_\omega}{T_\beta + T_\omega}$. The first transition represents an interaction (either infection or vaccination) between a susceptible and an infected node, which occurs with probability $(1 - \omega)\beta + \omega$. The Δ compartment represents an undetermined state. Then, in the second transition, the Δ node becomes infected with probability C_β or immunized with probability C_ω. Since the numbers of infected and vaccinated nodes come from the same Δ compartment, the transition probabilities C_ω and C_β determine the ratio between R and V at steady state:

$$\frac{V}{R} = \frac{C_\omega}{C_\beta} = \frac{T_\omega}{T_\beta} = \frac{\omega}{(1 - \omega)\beta}. \tag{5}$$

Note that both transitions in rule (4) occur within the same time step.

Analogously to the previous definitions of transmissibility, the first transition in rule (4) occurs with an effective probability $T_t = T_\beta + T_\omega$. Using this approach, the SIR-V can be mapped into mixed percolation, in which links and nodes are occupied with probability T_t and C_β, respectively. In our model, the order parameter, i.e., the fraction of recovered nodes, maps into the fraction P_∞ of nodes that belong to the
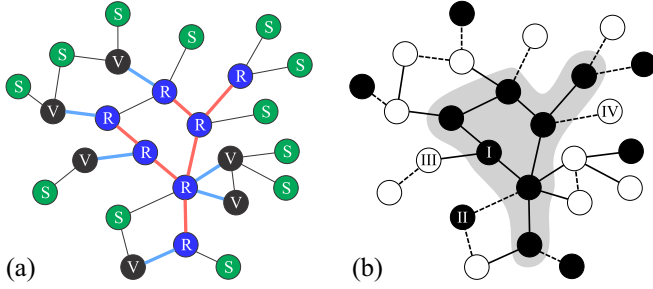
FIG. 1. Schematic illustration showing the equivalence between (a) the SIR-V and (b) the mixed percolation process. In (a), R-R links (red) were used to spread the disease, while R-V links (light blue) were used to immunize. In (b), the gray area indicates the GC. Node I belongs to the GC because it is occupied (filled circle) and has an occupied link (solid line) with the GC. This type of node is equivalent to a recovered node (R). In contrast, node II is occupied but its link that leads to the GC is not (dashed line). Thus, it is equivalent to a susceptible node (S) because there was no interaction through the link. Node III is not occupied (open circle), but its link with the GC is, so its equivalence is a vaccinated node (V). Finally, node IV (unoccupied site and link) is also equivalent to a susceptible node.

GC of the mixed percolation process. In this case, the GC is formed by occupied nodes connected by occupied links, as shown in Fig. 1. The control parameters T_t and C_β have the following expressions, as a function of β, ω, and t_r:

$$T_t = 1 - (1 - \omega)^{t_r}(1 - \beta)^{t_r}, \qquad (6)$$

$$C_\beta = \frac{(1 - \omega)\beta}{(1 - \omega)\beta + \omega}. \qquad (7)$$

In the following sections, we deduce analytical expressions for the fraction of recovered and vaccinated nodes, and subsequently we verify this mapping through stochastic simulations for different topologies.

III. THEORY FOR COMPLEX NETWORKS

Next, we use the generating function framework, which holds for networks that are locally trees [35]. The probability f_∞ of reaching an occupied node through a randomly chosen link that belongs to the GC of mixed percolation satisfies the self-consistent equation

$$f_\infty = C_\beta[1 - G_1(1 - T_t f_\infty)], \qquad (8)$$

where $G_1(x) = \sum_{k=k_{\min}}^{k_{\max}} kP(k)x^{k-1}/\langle k \rangle$ is the generating function of the excess degree distribution, for $x \in [0, 1]$. Here, k is the degree of a node, $P(k)$ is the degree distribution, $\langle k \rangle$ is the average degree, and $k_{\min}$ and $k_{\max}$ are the minimum and maximum degrees, respectively. Note that $G_1(1 - T_t f_\infty)$ is the probability that a branch does not expand to infinity and C_β the probability of occupying a node.

Equation (8) has a nontrivial solution depending on the control parameters. In the threshold value, only the null solution exists and the curves $y = f_\infty$ and $y = C_\beta[1 - G_1(1 - T_t f_\infty)]$ are tangent. Thus, this threshold can be found by differentiating both sides of Eq. (8) and

evaluating at $f_\infty = 0$,

$$1 = \frac{T_\beta}{T_t} \left. \frac{d[1 - G_1(1 - T_t f_\infty)]}{df_\infty} \right|_{f_\infty = 0},$$

where we replace $C_\beta = T_\beta/T_t$. Then

$$1 = T_{\beta_c} G_1'(1) \Rightarrow T_{\beta_c} = \frac{\langle k \rangle}{\langle k^2 \rangle - \langle k \rangle}.$$

Note that for an ER network, the variance equals $\langle k \rangle$, thus,

$$T_{\beta_c} = \frac{1}{\langle k \rangle}.$$

If $T_\beta > T_{\beta_c}$, Eq. (8) has a nontrivial solution and an epidemic phase can exist.

On the other hand, the fraction of recovered nodes R is equal to the probability that a randomly chosen node belongs to the GC in mixed percolation,

$$R = C_\beta[1 - G_0(1 - T_t f_\infty)], \qquad (9)$$

where $G_0(x) = \sum_{k=k_{\min}}^{k_{\max}} P(k)x^k$, for $x \in [0, 1]$, is the generating function of the degree distribution. Note that $[1 - G_0(1 - T_t f_\infty)]$ is the probability that at least one of its links is connected to the GC. On the other hand, for the fraction of vaccinated nodes V the expression is very similar, but the node must be unoccupied, which occurs with probability C_ω. Thus,

$$V = C_\omega[1 - G_0(1 - T_t f_\infty)]. \qquad (10)$$

The vaccinated nodes are part of the perimeter of the cluster of recovered nodes. If $\omega = 0$, the well-known mapping between the SIR process and link percolation is recovered. In addition, note that $\lim_{t_r \to \infty} T_t = 1$, so the only process that takes place in this limit is node percolation with parameter $C_\beta = T_\beta$.

Note that even though the fractions of recovered nodes R and vaccinated nodes V depend on the recovery time t_r [see Eqs. (6), (9), and (10)], their ratio does not, according to Eq. (5).

To check the validity of the previous equations, we choose some well-known network topologies (with a local treelike structure) and proceed to simulate the SIR-V process in them. As can be seen in Fig. 2, the simulation results agree well with the analytical results.

From our definition of the GC, we say that a node belongs to its perimeter if it does not belong to the GC but one of its neighbors does. There are three types of nodes that fulfill this condition in mixed percolation, which are represented in the schematic diagram in Fig. 3. Type I nodes (equivalent to vaccinated nodes) correspond to unoccupied nodes that have, at least, one occupied link connected to the GC. The probability of this event is given by Eq. (10). As for Types II and III nodes (equivalent to susceptible nodes), all their links that lead to the GC are unoccupied, i.e., they did not interact with its infected neighbors. This occurs with probability $G_0(1 - T_t f_\infty) - G_0(1 - f_\infty)$. A detailed derivation of these formulas is explained in the Appendix. By adding the fraction of nodes of Types I, II, and III, we obtain the expression for the fraction F of nodes in the perimeter of the GC:

$$F = 1 - C_\beta[1 - G_0(1 - T_t f_\infty)] - G_0(1 - f_\infty). \qquad (11)$$
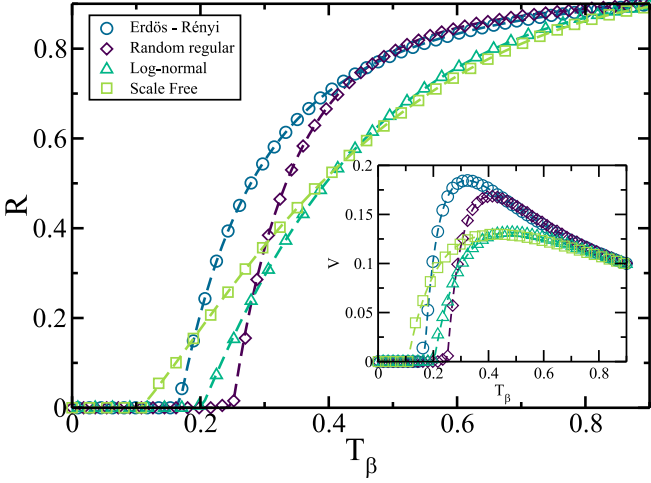
FIG. 2. Comparison between the simulation of the SIR-V process and the theoretical solutions for the number of recovered and vaccinated nodes. The epidemiological parameters used are $t_r = 1$ and $\omega = 0.1$. Note that the Erdös-Rényi (ER) and random regular (RR) types of networks are homogeneous, while the scale-free (SF) and log-normal (LN) networks are heterogeneous. For the ER network we use $\langle k \rangle = 6$, while for the RR network we use $k = 5$. For the SF network we choose an exponent of $\lambda = 2$ and opt for an exponential cutoff with parameter $c = 25$, while for the LN network the parameters are $\mu = 1$ and $\sigma = 0.7$. In all cases, $k_{\min} = 2$ and $k_{\max} = 250$.

For long recovery times $\lim_{t_r \to \infty} T_t = 1$, therefore, susceptible nodes do not contribute to F and only the term of vaccinated nodes remains:

$$F = C_\omega [1 - G_0(1 - f_\infty)]. \tag{12}$$

IV. WAXMAN SPATIAL NETWORK

We now turn our attention to Waxman-type networks, which cannot be studied with the generating function formalism because they are not locally trees. We consider $N = L^2$ nodes regularly distributed on a square of linear size L, with spacing $a = 1$. This choice differs from the model proposed in [26], where the nodes are uniformly distributed in the plane. Two nodes, i and j, are connected following the probability
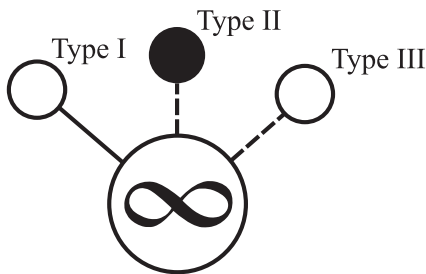

FIG. 3. Types of nodes in the perimeter of the GC of mixed percolation (equivalent to the cluster of recovered nodes). Filled and open circles represent occupied and unoccupied nodes, while solid and dashed lines represent occupied and unoccupied links, respectively.
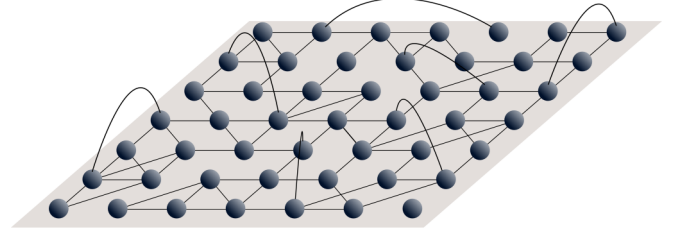

FIG. 4. Schematic diagram of a network built according to the Waxman model, where the length of the links follows an exponential distribution [Eq. (13)]. Circles represent nodes, which are arranged in a square lattice, while solid lines represent links of different lengths.

distribution

$$P_{ij} = c \exp(-r_{ij}/\xi), \tag{13}$$

where r_{ij} is the Euclidean distance between the nodes, c is a normalization factor, and ξ is a characteristic length. We restrict the domain of the function to $r \in [1, L/2]$, which is consistent with the choice of periodic boundary conditions. Thus, $c^{-1} = \xi[\exp(-\frac{1}{\xi}) - \exp(-\frac{L}{2\xi})]$. If L is large enough, the average connection distance tends to $\xi + 1$.

To build the network, we first choose a node i at random and generate two random numbers: one for the radius, according to the distribution defined in Eq. (13); and another for the angle, according to a uniform distribution between 0 and 2π. These two generated numbers define a radius vector. If we set its origin at the position of node i, the radius vector will point to a certain position in space. Then we choose the closest node to this position, say j, and connect i and j. This operation is repeated $N\langle k \rangle/2$ times, disallowing multiple connections, until the desired average connectivity $\langle k \rangle$ is obtained. In Fig. 4, we show a schematic diagram for $\xi = 1$; if ξ is set greater, the links become longer.

Due to the exponential decay, nodes mainly interact with neighbors in their nearby area. This area may be far from having a thermodynamic size, which would be the case for extremely long values of ξ. In Fig. 5(a), we plot the resulting degree distribution from the algorithm described in the previous paragraph. It can be seen that when the parameter ξ is small, the degree distribution has a binomial-type shape, which is consistent with the fact that the nearby area includes a few nodes. On the other hand, it can be seen that the distribution approaches a Poisson distribution as ξ grows. Similarly, it is expected that the clustering coefficient C [49], which accounts for the number of triangles in the network, may become considerable for small ξ and tend to 0 as ξ increases. The relationship between C and ξ is shown in Fig. 5(b).

Given that we are interested in the effect of different wiring costs on the spread of an epidemic, we focus on these networks (and ER networks, since they coincide in the limit of large ξ) to simulate the evolution of the SIR-V process.

V. RESULTS AND DISCUSSION

We perform stochastic simulations in Waxman networks of 10^6 nodes ($L = 10^3$), for different values of ω, β, t_r, and ξ. The average connectivity $\langle k \rangle$ was set to 4. We show in this
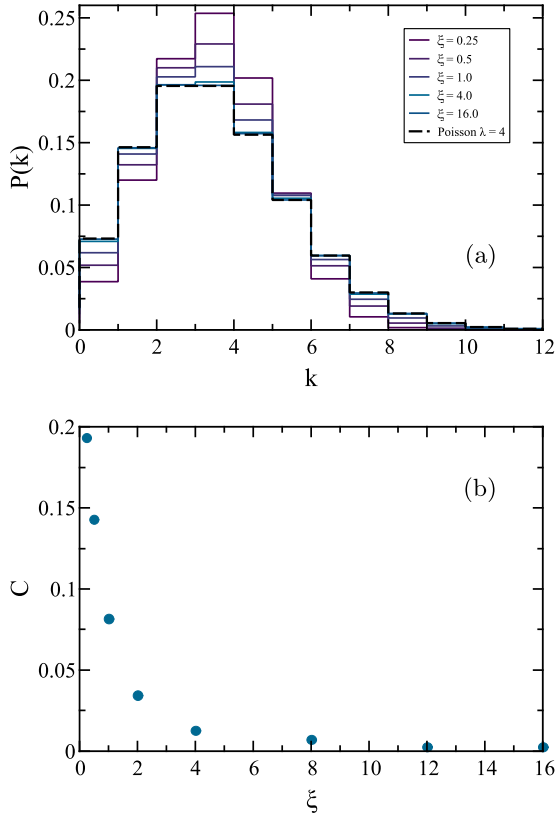
FIG. 5. Structural properties of the Waxman model. (a) Degree distribution of the nodes. (b) Network average clustering coefficient.

section that the mapping between the SIR-V model and mixed percolation holds for these spatial networks. In Sec. V A we focus on the fraction of recovered and vaccinated nodes at the final state, while in Sec. V B we present a phase diagram of the critical values that separate an epidemic phase from an epidemic-free phase. Finally, in Sec. V C we analyze the asymptotic case $t_r \to \infty$.

A. Extent of the epidemic

Here, we compute the fraction of recovered and vaccinated nodes of the SIR-V model from stochastic simulations. Following [50], we consider that the disease spreading in one realization results in an epidemic when the number of recovered nodes in the final state is above a threshold s_c. Below this threshold, only small outbreaks occur. Although our model is governed by two control parameters (T_t and C_β), here we show our results as a function of T_β because it is an effective probability of link-node occupation ($T_\beta = C_\beta T_t$, as mentioned in Sec. II), which summarizes the effect of link and node occupation probabilities on the order parameter in a mixed percolation process. Moreover, we see that this probability is useful to study the limit of node percolation in the SIR-V model (Sec. V C).

In Figs. 6 and 7, we show the fraction of vaccinated and recovered nodes for $\omega = 0.1$ and different values of ξ and t_r. As expected, higher transmissibility values T_β imply a greater extent of the epidemic, provided it is above a critical value $T_{\beta c}$. Below this value, ring vaccination halts the disease
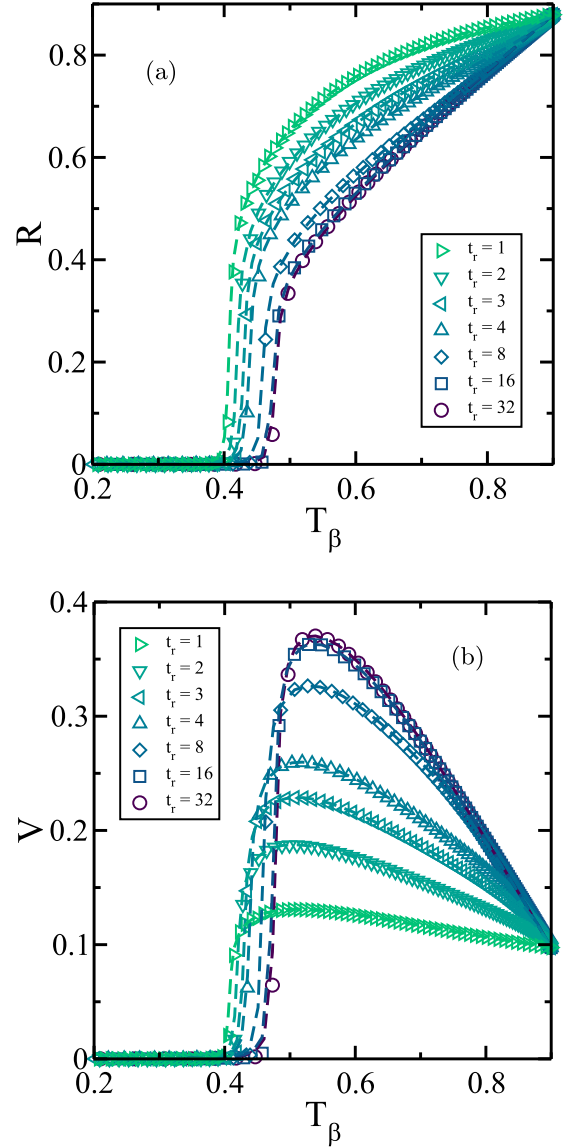

FIG. 6. Effect of varying t_r on the fraction of (a) recovered and (b) vaccinated nodes as a function of T_β, for $\xi = 1$, $\omega = 0.1$. The network has $N = 10^6$ nodes and the cutoff is $s_c = 300$. Different curves correspond to different values of t_r. Symbols represent the results of the SIR-V process, while dashed lines correspond to the results of mixed percolation.

spread and only small outbreaks occur. For low values of ξ, $T_{\beta c}$ increases with t_r, as shown in Fig. 6(a), in contrast to ER networks ($\xi \to \infty$), for which $T_{\beta c}$ does not depend on t_r. This observation proves that T_β cannot be a control parameter by itself, in contrast to [45], but it is not evident in complex networks. It is also observed that when t_r and T_β are large, the curve is almost linear, which is the typical form of node percolation (see Sec. V C). As for the fraction of vaccinated nodes, we show in Fig. 6(b) that it reaches notably higher values when the recovery time is longer. This complements the fact that the fraction of recovered nodes decreases with the recovery time, as shown in Fig. 6(a). To explain this result, note that since ω is fixed in Figs. 6(a) and 6(b), if t_r increases, then β must decrease to keep T_β constant [see Eq. (2)]. Also,
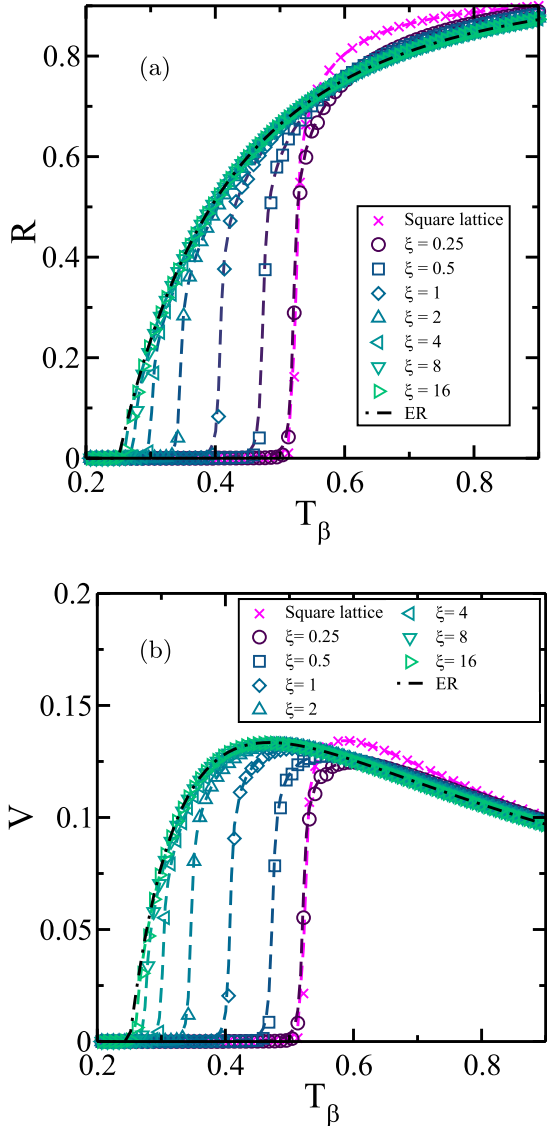
FIG. 7. Effect of varying ξ on the fraction of (a) recovered and (b) vaccinated nodes as a function of T_β, for $t_r = 1$, $\omega = 0.1$. The network has $N = 10^6$ nodes and the cutoff is $s_c = 300$. Different curves correspond to different values of ξ. Symbols represent the results of the SIR-V process, while dashed lines correspond to the results of mixed percolation. The first curve on the right (magenta ×'s) corresponds to a square lattice, for comparison, while the dash-dotted line on the left corresponds to the analytical solution for an ER network.

note from Eq. (5) that $T_\omega \propto T_\beta/\beta$, which implies that if β decreases, then the effective probability of vaccination T_ω increases. Therefore, if T_β remains constant, a longer recovery time enhances vaccination coverage. An interpretation of this observation is that a less virulent disease, even if it has a prolonged stage of infection, gives an advantage to the ring vaccination strategy. The existence of a peak in the curves of the fraction of vaccinated nodes is consistent with what is reported in [45] for ER and SF networks. This is due to competition between the spread of the disease and vaccination, as explained qualitatively in [45].
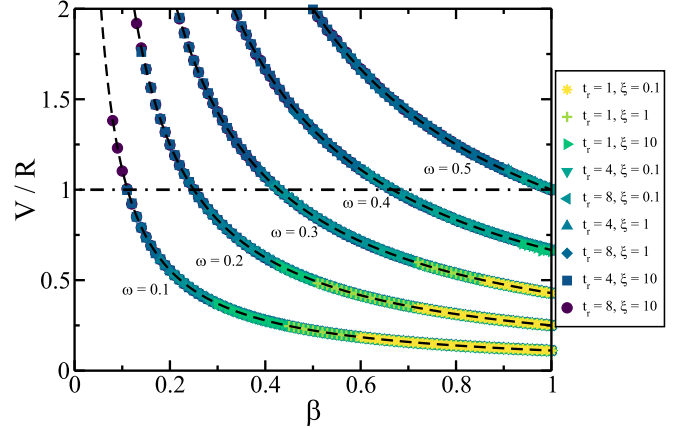

FIG. 8. Relation between the fraction of recovered and the fraction of vaccinated nodes as a function of β. Dashed lines represent Eq. (5). From left to right, the values used are $\omega = 0.1, 0.2, 0.3, 0.4,$ and 0.5. The different symbols are the numerical results for $t_r = 1$, 4, and 8 and $\xi = 0.1$, 1, and 10, in all possible combinations. The dash-dotted line indicates the case $V = R$.

In Figs. 7(a) and 7(b), it is shown that ξ has a strong influence on the critical value, which varies between the expected value for lattices ($T_{\beta c} = 0.5$) and that for ER networks ($T_{\beta c} = 0.25$). The longer the links, the more vulnerable to epidemics the network is. However, when the transmissibility is high (for $T_\beta \gtrsim 0.6$), networks with different values of ξ generate a similar fraction of recovered nodes in the final state and the extent of vaccination is similar.

Although Figs. 6 and 7 show that R and V depend on t_r and ξ, we expect from Eq. (5) that the ratio between them does not, regardless of the network topology. This is what we observe in Fig. 8 for Waxman networks with different values of ξ.

B. Phase diagram

The critical values that separate the epidemic phase from the epidemic-free phase can be considered the most significant results, since if the health agencies manage to keep diseases below these values, it means that they are under control. The values of β and t_r are associated with the disease, while ξ is determined by the social structure. The only parameter that health agencies can handle is the probability of immunization ω, allocating sufficient financial, logistic, and human resources to track the possible contacts of a patient and, then, convince them to get vaccinated. The values that must be achieved to avoid an epidemic can be found in the phase diagrams shown in Fig. 9. To summarize all cases of different recovery times, it is better to use C_β and T_t as parameters. Thus, the diagram is independent of the recovery time. Given C_β and T_t, we can obtain ω through Eqs. (2) and (3). To compute the critical value, we use the peak of the second-largest component.

C. Limit of long recovery times

As explained in Sec. III, when t_r is large enough, mixed percolation is dominated by node percolation. In this limit, $T_t = 1$ and $C_\beta = T_\beta$. Thus, the order parameter is governed
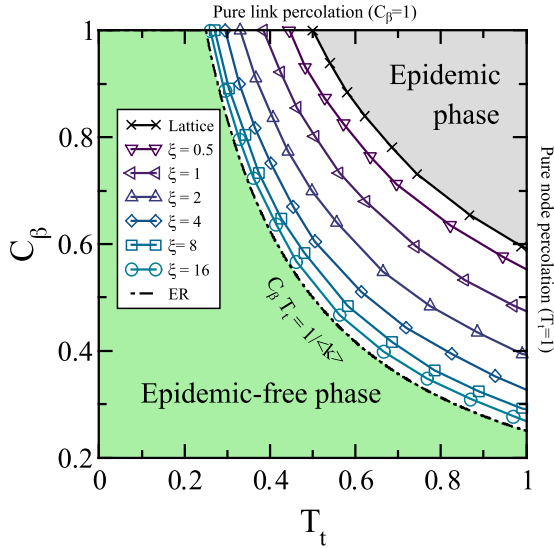
FIG. 9. Phase diagram. The different curves represent the critical values that separate the epidemic phase (above the curves) from the epidemic-free phase (below the curves) for different values of ξ. If $C_\beta = 1$ (top axis) the critical values correspond to link percolation, while if $T_t = 1$ (right axis) they correspond to node percolation. In the ER limit ($\xi \to \infty$), the product of C_β and T_t equals $\langle k \rangle^{-1}$.

only by T_β and the curves of the fraction of recovered or vaccinated nodes with different values of ω collapse into a single curve. The fraction of recovered nodes becomes linearly dependent with T_β (if $T_\beta \lesssim 1$), which is a characteristic behavior of node percolation, independently of the network topology and ω. In the case of complex networks, this linear behavior can be proved by expanding Eq. (9) in Taylor series to first order around $T_\beta = 1$:

$$R \approx 1 + [1 - G_0(1 - f_\infty)]|_{T_\beta = 1}(T_\beta - 1) = T_\beta.$$

Note that $f_\infty|_{T_\beta = 1} = 1$ and $G_0(0) = 0$. This behavior is very different from the SIR model and also contrasts with the results shown in Fig. 7(a), where there is no linear relation with T_β at any range.

In Fig. 10, the effects of different values of ξ are observed close to the critical values that separate the epidemic phase from the epidemic-free phase. As noted earlier, for sufficiently large transmissibility values, there is no difference in the extent of the epidemic, regardless of the length of the links.

In this limit, we obtain that the number of vaccinated nodes in the final state equals the perimeter of the cluster of recovered nodes (or, equivalently, to the perimeter of the GC in node percolation). That is, the disease is completely surrounded by vaccinated nodes. There are no susceptible nodes in contact with recovered nodes since there are so many chances of transmitting the disease from one node to another that the spread can only be stopped through immunization. Although this is valid in the limit of $t_r \to \infty$, as shown in Sec. III, we observe that for $t_r \sim 16$ the process is already strongly dominated by node percolation.

From the results presented, it can be seen that the stochastic simulations of the SIR-V model coincide very well with those of mixed percolation, verifying that this approach is valid.
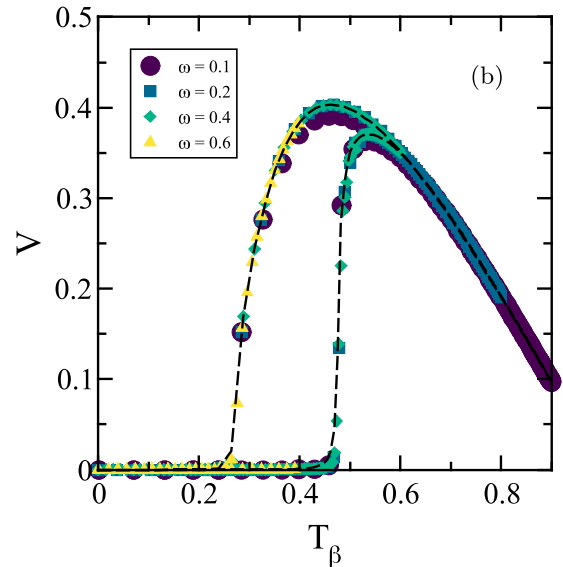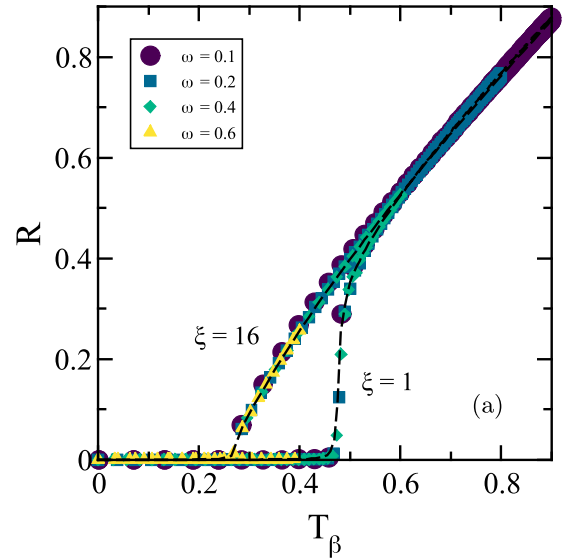

FIG. 10. (a) Recovered and (b) vaccinated nodes as a function of T_β in the limit of long recovery times. Symbols represent the results of the SIR-V process for $t_r = 16$, while dashed lines correspond to the magnitudes of pure node percolation: (a) fraction of nodes in the giant component (GC); (b) fraction of nodes in the perimeter of the GC. Different curves correspond to different values of ω.

VI. CONCLUSIONS

In this work we have studied an extension of the SIR model with ring vaccination, verifying the effectiveness of the strategy in spatial networks which were built according to the Waxman model, that is, in networks with distance-dependent connection costs. We found that there is an epidemic-free region that depends on the cost of connection and the recovery time of the disease. For high connection costs, the results are close to those expected for square lattices, where the network is more robust against diseases, while if the costs are negligible, the results approximate those expected for ER networks.

On the other hand, we showed that the fraction of recovered nodes of the epidemic process in the final state map into the relative size of the GC of the mixed percolation process. This process is controlled by two parameters, one corresponding to node percolation and the other to link percolation, which can be written as a function of the epidemiological parameters: β, ω, and t_r. Through the generating function formalism, we analytically derived the equations for the fraction of vaccinated and recovered nodes and computed the perimeter of the cluster of recovered nodes. In addition, we checked the mapping in Waxman spatial networks through numerical simulations and found that the ratio of recovered to vaccinated nodes is independent of the network topology.

Using the equivalence between the SIR-V model and mixed percolation, we show that for long recovery times (in practice, from $t_r \sim 16$ onwards) the results are dominated by node percolation. In this limit, the number of vaccinated nodes coincides with the total number of nodes in the perimeter of the cluster of recovered nodes, i.e., the disease only stops if it is surrounded by vaccinated individuals.

We believe that our results are important as they provide theoretical support for one of the most effective vaccination strategies, ring vaccination. Also, we show how its efficiency is related to the social structure, regarding short- and long-range interactions between people, which usually determines the extent of a disease.

Finally, regarding the current global pandemic, we would like to point out that this kind of model could be useful to study the spread of COVID-19. Even though a vaccine against the disease has not yet been developed, at least at the time of writing this paper, note that contact tracing of positive-tested individuals followed by quarantine works in a similar way to ring vaccination. Ideally, quarantined individuals cannot spread the disease as if they were immunized, although they could be infected. In addition, recent research has suggested that the spatial spread of coronavirus in China is strongly related to the spatial network of interurban migration [51]. Thus, further studies are needed to understand the impact of spatial networks on strategies to halt the spread of a disease. All in all, we believe that approaches like our SIR-V model could be a useful tool to analyze the spread of several infectious diseases such as COVID-19.

APPENDIX: DETAILED DEDUCTION OF THE EQUATION FOR THE PERIMETER OF THE MIXED PERCOLATION CLUSTER

In a mixed percolation of nodes and links, there are three types of nodes that can be part of the perimeter of the infinite cluster. Type I nodes arise from the node percolation process, Type II nodes correspond to the link percolation process, and Type III nodes are exclusive of mixed percolation. In the following subsections, we compute the fraction of these nodes
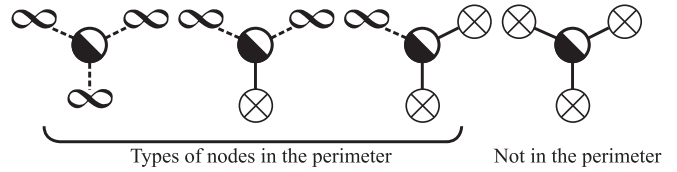

FIG. 11. Possible connections of Type II or III nodes. The central circles are half-filled because they represent either occupied or unoccupied nodes, while solid and dashed lines represent occupied and unoccupied links, respectively. If the link leads to the GC (represented by the ∞ symbol) it must be unoccupied. On the other hand, the $\otimes$ symbol represents all cases that are not the giant component.

for complex networks. As we only use percolation theory arguments, we denote p_N and p_L the control parameters of node and link percolation, respectively, and P_∞ the order parameter.

1. Type I nodes

Type I nodes are unoccupied with at least one occupied link that connects them with the GC. As stated before, in the context of the SIR-V model an occupied link represents an interaction between an infected and a susceptible node. Since Type I nodes are unoccupied, they correspond to vaccinated nodes. Accordingly, we can write the probability of choosing a Type I node as

$$(1 - p_N)[1 - G_0(1 - p_L f_\infty)]. \tag{A1}$$

2. Types II and III nodes

Types II and III are nodes with at least one link leading to the GC, but it is "unoccupied," while the rest of the links connect to nodes that do not belong to the GC. In Fig. 11 we show a schematic diagram of the possible configurations of these two types of nodes, for a random regular network with degree $k = 3$.

The probability that a randomly chosen link leads to the GC is f_∞. In this case, the link must be unoccupied, which occurs with probability $(1 - p_L)$. For example, for a random regular with $k = 3$, the probability of choosing a Type II or III node is proportional to

$$[(1 - p_L)f_\infty]^3 + 3[(1 - p_L)f_\infty]^2(1 - f_\infty)$$
$$+ 3[(1 - p_L)f_\infty](1 - f_\infty)^2,$$

where the prefactors in each term account for the possible permutations (see Fig. 11). If all nodes have a k degree, the last expression can be written as

$$\sum_{j=1}^{k} C_k^j [(1 - p_L)f_\infty]^j (1 - f_\infty)^{k-j}$$
$$= (1 - p_L f_\infty)^k - (1 - f_\infty)^k,$$

where C_k^j is the binomial coefficient.

In order to consider any degree distribution, we have to take into account the probability of having a degree k and sum over all cases, so the last expression takes the more general form

$$\sum_{k=k_{\min}}^{k_{\max}} P(k)[(1-p_L f_\infty)^k - (1-f_\infty)^k]$$

$$= G_0(1-p_L f_\infty) - G_0(1-f_\infty). \quad (A2)$$

The last expression should be multiplied by the node percolation parameter p_N if we only consider occupied sites (Type II) or by $(1-p_N)$ in the case of unoccupied sites (Type III). But if we add Types II and III contributions, we obtain Eq. (A2).

3. Total expression for perimeter sites

By adding all the terms deduced in the previous sections, i.e., Eqs. (A1) and (A2), we obtain the expression for the fraction of sites in the perimeter of the GC:

$$F = (1-p_N)[1-G_0(1-p_L f_\infty)]$$

$$+ G_0(1-p_L f_\infty) - G_0(1-f_\infty).$$

After some algebra, the last expression can be rewritten in a more intuitive way:

$$F = 1 - p_N[1-G_0(1-p_L f_\infty)] - G_0(1-f_\infty). \quad (A3)$$

The last term accounts for the fraction of nodes that are not in the GC or in its perimeter (see Fig. 11; fourth case). Also, note that the second term corresponds to P_∞, i.e., the fraction of nodes in the GC. Thus,

$$F = 1 - P_\infty - G_0(1-f_\infty). \quad (A4)$$

[1] K. Xu, A. Soucat, J. Kutzin, C. Brindley, N. Vande Maele, H. Toure, M. Aranguren Garcia, D. Li, H. Barroy, G. Flores Saint-Germain, T. Roubal, C. Indikadahena, and V. Cherilova, *Public Spending on Health: A Closer Look at Global Trends* (World Health Organization, Geneva, Switzerland, 2018).

[2] World Health Organization, *Managing Epidemics: Key Facts About Major Deadly Diseases* (World Health Organization, Geneva, Switzerland, 2018).

[3] S. Boccaletti, V. Latora, Y. Moreno, M. Chavez, and D. Hwang, Phys. Rep. **424**, 175 (2006).

[4] R. Cohen and S. Havlin, *Complex Networks: Structure, Robustness and Function* (Cambridge University Press, Cambridge, UK, 2010).

[5] A. Barrat, M. Barthélemy, R. Pastor-Satorras, and A. Vespignani, Proc. Natl. Acad. Sci. USA **101**, 3747 (2004).

[6] M. E. J. Newman, *Networks: An Introduction* (Oxford University Press, New York, 2010).

[7] C. Castellano and R. Pastor-Satorras, Phys. Rev. Lett. **105**, 218701 (2010).

[8] R. Pastor-Satorras, C. Castellano, P. Van Mieghem, and A. Vespignani, Rev. Mod. Phys. **87**, 925 (2015).

[9] M. De Domenico, C. Granell, M. A. Porter, and A. Arenas, Nat. Phys. **12**, 901 (2016).

[10] W. Wang, M. Tang, H. E. Stanley, and L. A. Braunstein, Rep. Prog. Phys. **80**, 036603 (2017).

[11] R. M. Anderson and R. M. May, *Infectious Diseases of Humans: Dynamics and Control* (Oxford University Press, Oxford, UK, 1992).

[12] N. T. J. Bailey, *The Mathematical Theory of Infectious Diseases* (Griffin, London, 1975).

[13] C. Fraser, S. Riley, R. M. Anderson, and N. M. Ferguson, Proc. Natl. Acad. Sci. USA **101**, 6146 (2004).

[14] B. Pourbohloul, L. A. Meyers, D. M. Skowronski, M. Krajden, D. M. Patrick, and R. C. Brunham, Emerging Infect. Dis. **11**, 1249 (2005).

[15] T. Day, A. Park, N. Madras, A. Gumel, and J. Wu, Am. J. Epidemiol. **163**, 479 (2006).

[16] N. M. Ferguson, D. A. Cummings, C. Fraser, J. C. Cajka, P. C. Cooley, and D. S. Burke, Nature **442**, 448 (2006).

[17] L. G. Alvarez-Zuzek, H. E. Stanley, and L. A. Braunstein, Sci. Rep. **5**, 12151 (2015).

[18] L. G. Alvarez-Zuzek, C. Buono, and L. A. Braunstein, J. Phys.: Conf. Ser. **640**, 012007 (2015).

[19] Z. Wang, C. T. Bauch, S. Bhattacharyya, A. d'Onofrio, P. Manfredi, M. Perc, N. Perra, M. Salathé, and D. Zhao, Phys. Rep. **664**, 1 (2016).

[20] R. Pastor-Satorras and A. Vespignani, Phys. Rev. E **65**, 036104 (2002).

[21] N. Madar, T. Kalisky, R. Cohen, D. ben-Avraham, and S. Havlin, Eur. Phys. J. B **38**, 269 (2004).

[22] R. Cohen, S. Havlin, and D. Ben-Avraham, Phys. Rev. Lett. **91**, 247901 (2003).

[23] J. V. Noble, Nature **250**, 726 (1974).

[24] D. Brockmann, *Reviews of Nonlinear Dynamics and Complexity* (John Wiley & Sons, Hoboken, NJ, 2010), Chap. 1, pp. 1–24.

[25] B. M. Waxman, IEEE J. Sel. Areas Commun. **6**, 1617 (1988).

[26] M. Barthélemy, Phys. Rep. **499**, 1 (2011).

[27] S. Horvát, R. Gămănut, M. Ercsey-Ravasz, L. Magrou, B. Gămănut, D. C. Van Essen, A. Burkhalter, K. Knoblauch, Z. Toroczkai, and H. Kennedy, PLoS Biol. **14**, e1002512 (2016).

[28] A. Fornito, A. Zalesky, and E. Bullmore, *Fundamentals of Brain Network Analysis* (Academic Press, San Diego, CA, 2016).

[29] R. Lambiotte, V. D. Blondel, C. De Kerchove, E. Huens, C. Prieur, Z. Smoreda, and P. Van Dooren, Physica A: Stat. Mech. Appl. **387**, 5317 (2008).

[30] E. W. Zegura, K. L. Calvert, and S. Bhattacharjee, in *Proceedings of IEEE INFOCOM'96. Conference on Computer Communications* (IEEE, New York, 1996), Vol. 2, pp. 594–602.

[31] P. Hines, S. Blumsack, E. C. Sanchez, and C. Barrows, in *2010 43rd Hawaii International Conference on System Sciences* (IEEE, New York, 2010), pp. 1–10.

[32] I. Bonamassa, B. Gross, M. M. Danziger, and S. Havlin, Phys. Rev. Lett. **123**, 088301 (2019).

[33] P. Erdös and A. Rényi, Publ. Math. Debrecen **6**, 290 (1959).

[34] Y. Moreno, R. Pastor-Satorras, and A. Vespignani, Eur. Phys. J. B **26**, 521 (2002).

[35] M. E. J. Newman, Phys. Rev. E **66**, 016128 (2002).

[36] L. D. Valdez, P. A. Macri, and L. A. Braunstein, PLoS ONE **7**, e44188 (2012).

[37] L. D. Valdez, P. A. Macri, and L. A. Braunstein, Physica A: Stat. Mech. Appl. **392**, 4172 (2013).

[38] V. Colizza, A. Barrat, M. Barthélemy, and A. Vespignani, BMC Med. **5**, 34 (2007).

[39] P. Grassberger, Math. Biosci. **63**, 157 (1983).

[40] S. Merler, M. Ajelli, L. Fumanelli, S. Parlamento, A. Pastore y Piontti, N. E. Dean, G. Putoto, D. Carraro, I. M. Longini Jr., M. E. Halloran *et al.*, PLoS Neglected Trop. Dis. **10**, e0005093 (2016).

[41] P.-S. Gsell, A. Camacho, A. J. Kucharski, C. H. Watson, A. Bagayoko, S. D. Nadlaou, N. E. Dean, A. Diallo, A. Diallo, D. A. Honora *et al.*, Lancet Infect. Dis. **17**, 1276 (2017).

[42] M. A. Strassburg, Am. J. Infect. Control **10**, 53 (1982).

[43] F. Fenner, D. A. Henderson, I. Arita, Z. Jezek, I. D. Ladnyi *et al.*, *Smallpox and Its Eradication* (World Health Organization, Geneva, Switzerland, 1988), Vol. 6.

[44] World Health Organization, *Preliminary Results on the Efficacy of rVSV-ZEBOV-GP Ebola Vaccine Using the Ring Vaccination Strategy in the Control of an Ebola Outbreak in the Democratic Republic of the Congo: An Example of Integration of Research into Epidemic Response* (World Health Organization, Geneva, Switzerland, 2019).

[45] L. G. Alvarez-Zuzek, M. A. Di Muro, S. Havlin, and L. A. Braunstein, Phys. Rev. E **99**, 012302 (2019).

[46] M. A. Di Muro, L. G. Alvarez-Zuzek, S. Havlin, and L. A. Braunstein, New J. Phys. **20**, 083025 (2018).

[47] J. Hammersley and D. Welsh, Contemp. Phys. **21**, 593 (1980).

[48] D. S. Callaway, M. E. J. Newman, S. H. Strogatz, and D. J. Watts, Phys. Rev. Lett. **85**, 5468 (2000).

[49] D. J. Watts and S. H. Strogatz, Nature **393**, 440 (1998).

[50] C. Lagorio, M. V. Migueles, L. A. Braunstein, E. López, and P. A. Macri, Physica A **388**, 755 (2009).

[51] B. Gross, Z. Zheng, S. Liu, X. Chen, A. Sela, J. Li, D. Li, and S. Havlin, medRxiv 2020.03.23.20041517 (2020).